



HAL
open science

Characterization of TCL, a New GTPase of the Rho Family related to TC10 and Cdc42

Emmanuel Vignal, Marion de Toledo, Franck Comunale, Angela Ladopoulou, Cécile Gauthier-Rouvière, Anne Blangy, Philippe Fort

► **To cite this version:**

Emmanuel Vignal, Marion de Toledo, Franck Comunale, Angela Ladopoulou, Cécile Gauthier-Rouvière, et al.. Characterization of TCL, a New GTPase of the Rho Family related to TC10 and Cdc42. *Journal of Biological Chemistry*, 2000, 275 (46), pp.36457-36464. 10.1074/jbc.M003487200 . hal-02267476

HAL Id: hal-02267476

<https://hal.science/hal-02267476>

Submitted on 26 Jun 2020

HAL is a multi-disciplinary open access archive for the deposit and dissemination of scientific research documents, whether they are published or not. The documents may come from teaching and research institutions in France or abroad, or from public or private research centers.

L'archive ouverte pluridisciplinaire **HAL**, est destinée au dépôt et à la diffusion de documents scientifiques de niveau recherche, publiés ou non, émanant des établissements d'enseignement et de recherche français ou étrangers, des laboratoires publics ou privés.

Characterization of TCL, a New GTPase of the Rho Family related to TC10 and Cdc42*[§]

Received for publication, April 25, 2000, and in revised form, July 25, 2000
Published, JBC Papers in Press, August 30, 2000, DOI 10.1074/jbc.M003487200

Emmanuel Vignal[¶], Marion De Toledo[¶], Franck Comunale[‡], Angela Ladopoulou^{||},
Cécile Gauthier-Rouvière[‡], Anne Blangy[‡], and Philippe Fort^{‡**}

From the [‡]Centre de Recherche en Biochimie Macromoléculaire, CNRS-UPR 1086, 1919 Route de Mende, 34293 Montpellier cedex 5, France and the ^{||}Molecular Diagnostics Laboratory, Institute of Radioisotopes & Radiodiagnostic Products National Center for Scientific Research "Demokritos," 15310 Athens, Greece

GTPases of the Rho family control a wide variety of cellular processes such as cell morphology, motility, proliferation, differentiation, and apoptosis. We report here the characterization of a new Rho member, which shares 85% and 78% amino acid similarity to TC10 and Cdc42, respectively. This GTPase, termed as TC10-like (TCL) is encoded by an unexpectedly large locus, made of five exons spanning over 85 kilobases on human chromosome 14. TCL mRNA is 2.5 kilobases long and is mainly expressed in heart. *In vitro*, TCL shows rapid GDP/GTP exchange and displays higher GTP dissociation and hydrolysis rates than TC10. Using the yeast two-hybrid system and GST pull-down assays, we show that GTP-bound but not GDP-bound TCL protein directly interacts with Cdc42/Rac interacting binding domains, such as those found in PAK and WASP. Despite its overall similarity to TC10 and Cdc42, the constitutively active TCL mutant displays distinct morphogenic activity in REF-52 fibroblasts, producing large and dynamic F-actin-rich ruffles on the dorsal cell membrane. Interestingly, TCL morphogenic activity is blocked by dominant negative Rac1 and Cdc42 mutants, suggesting a cross-talk between these three Rho GTPases.

The Rho GTPases form a distinct family of the Ras superfamily of low molecular weight GTP-binding proteins. Rho proteins are key elements in the regulation of dynamic assembly of cytoskeletal components, that participate in physiological processes such as cell proliferation and motility, establishment of cell polarity (reviewed in 1), as well as in physiopathological processes such as cell transformation and metastasis (2, 3). The

Rho family is made of two main groups. One comprises Rho(A–C), RhoD, Rnd(1–3), and RhoL; the other comprises Rac(1–3), RhoG, Cdc42, TC10, TTF/RhoH, and Chp (reviewed in Ref. 4). In fibroblastic cells, Rho(A–C) control the formation of focal adhesions and actin stress fiber bundling (5, 6), while RhoD causes rearrangements of the actin cytoskeleton and controls early endosome motility and distribution (7). Cdc42 and TC10 regulate the formation of filopodia (8, 9), while Rac proteins are required for growth factor-induced membrane ruffling and lamellipodia formation (5). In neurons, Rho proteins are required for axonal outgrowth (10), while in phagocytic cells, they play a role in the activation of NADPH oxidase (11), the polarization of helper T cells toward antigen-presenting cells (12), and apoptosis (13).

Like other Ras-related proteins, Rho GTPases adopt either an active GTP-bound or an inactive GDP-bound conformational state. Their activity is controlled positively by guanine nucleotide exchange factors, which catalyze the replacement of GDP with GTP, and negatively by GTPase-activating proteins, which accelerate the endogenous GTPase activity (14). Once loaded with GTP, the GTPase binds to and activates a set of downstream effector proteins directly or indirectly involved in the initiation of the cellular effects (reviewed in Ref. 15). Activation or inhibition of different Rho GTPases have been reported to control the formation of similar F-actin-containing structures, which might be a consequence of two distinct mechanisms. First, this might result from activation cascades involving several GTPases. This is the case for Cdc42, whose activation promotes the formation of filopodia as well as Rac-dependent lamellipodia (6); for RhoG, which promotes the formation of filopodia and lamellipodia through Rac1 and Cdc42 activities (16); and for RhoA, whose inactivation leads to the downstream activation of Rac1 and Cdc42 (17). Second, distinct GTPases might activate identical downstream effector proteins. This might be the case for Cdc42 and TC10, which share several effectors and both trigger the formation of filopodial extensions (9).

It thus emerges that identifying all GTPases of the Rho family is an essential step toward understanding how these proteins act in concert in the control of cell physiology. Here we report the identification of a new Rho member in mammals, based on its homology with Cdc42 and TC10. Sequence analysis indicates that this new protein, termed as TCL, is encoded by a 2.5-kb¹ mRNA preferentially expressed in heart. Like TC10 and Cdc42, TCL binds Cdc42/Rac interacting binding (CRIB)

* This work was supported by grants from the Ligue Nationale Contre le Cancer and in part by the Association pour la Recherche contre le Cancer. The costs of publication of this article were defrayed in part by the payment of page charges. This article must therefore be hereby marked "advertisement" in accordance with 18 U.S.C. Section 1734 solely to indicate this fact.

[§] The on-line version of this article (available at <http://www.jbc.org>) contains videos of dynamic structures elicited by GFP-TCL_{Q79L} and GFP-TC10_{Q75L}. REF-52 cells were transfected to express GFP-TCL_{Q79L} (panel a) and GFP-TC10_{Q75L} (panel b). 18 h after transfection, GFP-positive cells were examined for 10 min by time-lapse microscopy (400-ms exposure time every 10 s). Cell images were captured (400 ms) as time series of 16-bit files. Selected images were assembled as video movies using Quicktime (version 4.0).

The nucleotide sequence(s) reported in this paper has been submitted to the GenBank™/EBI Data Bank with accession number(s) AJ276567 and AJ276568.

[¶] Supported by a fellowship from the Ministère de l'Éducation Nationale et de la Recherche (France).

^{||} These two authors contributed equally to this work.

** To whom correspondence should be addressed. Tel.: 33-467613356; Fax: 33-467521559; E-mail: fort@crbm.cnrs-mop.fr.

¹ The abbreviations used are: kb, kilobase(s); GTPγS, guanosine 5'-3-O-(thio)triphosphate; CRIB, Cdc42/Rac interacting binding; SE, scanning electron microscopy; EST, expressed sequence tag; bp, base pair(s); GST, glutathione S-transferase; MBP, maltose-binding protein; PCR, polymerase chain reaction; GFP, green fluorescent protein; ORF, open reading frame; UK, United Kingdom.

domains of PAK and WASP. However, expression of the constitutively active TCL and TC10 proteins elicits the formation of distinct cytoskeletal structures in fibroblasts.

EXPERIMENTAL PROCEDURES

Data Base Search—Searches in human and murine data bases for sequences homologous to TC10 cDNA were done using BLAST (18) and ENTREZ NCBI web facilities. One human genomic sequence was identified (AL049871.2) as well as human ESTs (AA020825, AA020848, AA424648, AA434363, AA461242, AA920345, AI066690, AI091480, AI366101, AI369275, AI370786, AI378515, AI583530, N27528, N40345, and W59948), and murine ESTs (AA051640, AA537565, AI182685, AI322267, AI462525, AI510273, AI920345, AI931399, AW060455, AW121127, W10994, W12115, and W16055). Human- and mouse-derived TCL protein sequences were aligned with other Rho GTPases using MULTALIN (19). Distance matrices were computed and used to draw a similarity tree using ClustalW (20) and Treeview (21).

Constructs—IMAGE clones 269952 and 363723 (human) and 1383415 and 316263 (mouse) containing TCL full-length cDNAs were obtained from the United Kingdom (UK) Human Genome Mapping Project Resource Center (Cambridge, UK). The human TCL open reading frame (ORF) was amplified by PCR and cloned in pBlueScript KS. Q79L and T35N mutations were introduced using the Gene Editor kit (Promega). The CAAX box was deleted by *PvuII* cleavage. The original clones as well as wild-type and mutated PCR fragments were fully sequenced. Wild-type and mutated ORFs were subcloned in prokaryotic pGEX-4T-2 vector (Life Science), yeast pBTM116, and mammalian pEGFP-C2 (CLONTECH). PAK-1 ORF was obtained by PCR amplification and subcloned in pGAD1318. WASP fragment (amino acids 201–321) containing the CRIB domain was swapped from pGEX-KG to pGAD1318. pGAD1318-Kinectin (clone 66, encoding amino acids 677–913) was isolated from an interaction screen with RhoG (16). pGEX-PAK expressing GST protein fused to human PAK1B CRIB domain (amino acids 5–131) was kindly provided by Anja Bathoorn (Netherlands Cancer Institute, Amsterdam, Netherlands). For *in vitro* interaction purposes, the insert containing PAK1B CRIB domain was swapped from pGex to pMal-C2 vector (New England Biolabs). pGEX-WASP and pActII-ROCK (encoding amino acids 888–1030) were kindly provided by A. Hall (University College, London, UK).

Recombinant TCL Purification and Antibody Production—GST-TCLwt and GST-TC10wt were expressed in *E. coli* using the pGEX vectors according to standard procedures. Briefly, bacteria were grown to mid log phase at 25 °C and then induced with 0.3 mM IPTG for 2.5 h at 25 °C. Bacteria were then pelleted; washed; re-suspended in PBS containing 1 mM phenylmethylsulfonyl fluoride, 1 mM MgCl₂, 1 mM dithiothreitol, 100 μM GDP, and lysozyme (0.25 mg·ml⁻¹); incubated on ice for 1 h; and sonicated. Insoluble material was removed by centrifugation. 300 μl of glutathione-S-Sepharose 4B beads (Amersham Pharmacia Biotech) were added to the cleared lysate, incubated for 30 min at 4 °C, and washed three times in PBS. GST fusion proteins were eluted twice in 50 mM Hepes-NaOH (pH 7.5) containing 10 mM dithiothreitol, 1 mM MgCl₂, 1 μM GDP, and 20 mM reduced glutathione (Sigma). Recombinant GST-TCL was further used for biochemical studies and for raising antibodies. Rabbits were submitted to three rounds of injection of 0.1 mg of GST-TCL. Immunosera were depleted on GST-bound Sepharose, then affinity-purified on GST-TCL-bound Sepharose.

Exchange and GTP Hydrolysis Assays—For loading assays, 1 μM GTPase was incubated with 10 μM nucleotide ([³⁵S]GTPγS or [³H]GDP) in Load Buffer (50 mM Hepes-NaOH (pH 7.4), 100 mM KCl, 2 mM MgCl₂, and 1 mM dithiothreitol). For off-rate measurements, 1 μM GST-GTPases was incubated for 2 min at 37 °C with 10 μM nucleotide [³⁵S]GTPγS in MgCl₂-free Load Buffer. Nucleotide exchange was started by adding 2 mM MgCl₂ and 1 mM unlabeled GTP. For loading and exchange kinetics, 25-μl aliquots (25 pmol) were taken at different times, added to 25 μl of cold "Stop Buffer" (50 mM Tris-HCl (pH 7.5), 10 mM MgCl₂), and filtered on 0.45-μm membranes (Schleicher & Schuell). *k*_{off} values were calculated assuming single-exponential kinetics. For GTP hydrolysis assays, GST-GTPases were loaded for 2 min at 37 °C with 10 μM [³²P]GTP in MgCl₂-free Load Buffer supplemented with 5 mM P_i. GTP hydrolysis was started by adding 2 mM MgCl₂. 25-μl aliquots were taken out at different times, mixed with 975 μl of charcoal in 50 mM NaH₂PO₄, and centrifuged. ³²P_i release was measured by counting the supernatant.

RNA Hybridization—Mouse MTN blot (CLONTECH) was pre-hybridized for 30 min. at 65 °C in 5 ml of ExpressHyb buffer (CLONTECH), then hybridized for 1 h at 65 °C in the same buffer containing denatured [^α-³²P]dCTP-labeled murine probe (1–2 × 10⁶ cpm·ml⁻¹).

Filter was then washed twice for 15 min at 65 °C in 50 ml of 2× SSC, 0.1% SDS, and once for 15 min at 52 °C in 50 ml of 0.2× SSC, 0.1% SDS. Filter was sequentially hybridized with TCL and β-actin cDNA probes.

Two-hybrid and in Vitro Interaction Analysis—For interaction studies in yeast, pBTM116 constructs expressing dominant active TCL_{Q79L} or dominant negative TCL_{T35N} mutants as well as dominant active TC10_{Q75L} and dominant active Cdc42_{G12V} fused to LexA DNA binding domain were cotransformed in TAT-7 strain with plasmids expressing PAK, WASP, or kinectin fused to Gal4 activating domains, as described previously (22). Double transformants were selected on drop-out medium lacking leucine and tryptophan and assayed for β-galactosidase activity.

For *in vitro* interaction studies, 10 μg of GST-TCL (0.2 nmol) bound to Glutathione Sepharose was loaded for 2 min. at 37 °C in 100 μl of magnesium-free Load Buffer supplemented with 1 mM GTPγS or GDP, then blocked by adding 20 mM MgCl₂. Under these conditions, 20% of TCL was loaded with GTP. The GTPase was then incubated on ice for 2 h with 15 μg of maltose-binding protein (MBP) (0.35 nmol) or MBP-CRIB (0.3 nmol), 1 mg·ml⁻¹ bovine serum albumin, 0.1% Tween 20. Sepharose beads were rinsed three times in ice-cold Load Buffer supplemented with 1 mg·ml⁻¹ bovine serum albumin, 0.1% Tween 20. Total and Sepharose-bound proteins were denatured in Laemmli buffer and then analyzed by Western blotting using anti-MBP and anti-TCL antibodies.

Cell Culture and Transfection—Rat embryo fibroblasts (REF-52) and human 293 (Bosc) cells were cultured at 37 °C in the presence of 5% CO₂ in Dulbecco's modified Eagle's medium supplemented with 10% fetal calf serum. Cells were plated on 18-mm diameter glass coverslips 16–24 h before transfection. Cells were transfected using the LipofectAMINE method, as described by the supplier (Life Technologies, Inc.). Four hours after the transfection, the medium was replaced by Dulbecco's modified Eagle's medium supplemented with 10% fetal calf serum. Expressing cells were observed under fluorescence microscopy 8–24 h after transfection.

GST-CRIB Pull-down Assay—Interactions were performed as described by Sander *et al.* (23). Bosc cells were transfected with constructs expressing enhanced green fluorescent protein (GFP) alone (CLONTECH) or fused to the constitutive active mutants of Cdc42, RhoG, TC10, and TCL. 24 h after transfection, cells were rapidly washed in ice-cold PBS and lysed on ice in 50 mM Tris-HCl (pH 7.4), 2 mM MgCl₂, 1% Triton X-100, 10% glycerol, 100 mM NaCl, and protein inhibitor mixture. Lysates were centrifuged for 5 min at 17,000 × *g* at 4 °C, and samples were taken from the supernatant to estimate total protein concentration. 20 μg of GST-CRIB fusion bound to Sepharose beads were added to cell lysate and incubated for 30 min at 4 °C. Beads were washed four times in lysis buffer, and bound proteins were eluted in Laemmli sample buffer. Total proteins and CRIB affinity-purified proteins were analyzed by Western blotting using a monoclonal antibody directed against GFP (CLONTECH).

Immunohistochemistry—Cells were fixed for 5 min in 3.7% formalin (in PBS) followed by a 2-min permeabilization with 0.1% Triton X-100 (in PBS) and incubation in PBS containing 0.1% bovine serum albumin. Expression of GFP-tagged proteins was directly visualized. F-actin was revealed using rhodamine-conjugated phalloidin (0.5 unit·ml⁻¹; Sigma). Expression of Myc epitope-tagged proteins was visualized after a 60-min incubation with the 9E10 anti-Myc mAb or 12CA5 anti-HA mAb, followed by incubation with affinity purified 7-amino-4-methylcoumarin-3-acetic acid-conjugated donkey anti-mouse IgG (1:50 dilution, Jackson Immunoresearch Laboratories, West Grove, PA). Cells were washed in PBS, mounted in Mowiol (Aldrich), and observed under microscopy.

Cell Imaging—Cell imaging was performed at the Integrated Imaging Facility of the laboratory. The microscopes were all Leicas (Leica, Wetzlar, Germany) with PL APO grade oil objectives. Images were captured as 16 TIFF files with MicroMax 1300 Y/HS (B/W) cooled (–10 °C) CCD cameras (RS-Princeton Instruments Inc.) driven by MetaMorph (version 4.11; Universal Imaging Corp.). MetaMorph also driven built-in microscope shutters and piezoelectric stepping motors (PZ 73E) attached to the lens turret through an E-662 LVPZT servo controller (Physik Instrument, Waldbronn, Germany). Rhodamine fluorescence was observed a N2.1 cube filter and GFP fluorescence with a GFP cube filter (Leica). For cell fluorescence quantitation, a 63× (numeric aperture, 1.32) and a constant time exposure (400 ms) were used. Cell fluorescence was measured after thresholding using the View Region Statistics module of MetaMorph. For all experiments, at least 100 transfected cells were examined, unless stated in the text.

Three-dimensional Analysis of F-actin Cell Distribution—To examine inner cell three-dimensional F-actin organization, stacks of optical sections (*z* step = 0.088 μm) were captured with a DMR B microscope

using a 63× (numeric aperture, 1.32) objective mounted on a piezoelectric stepping motor. Stacks were first restored with Huygens (Scientific Volume Imaging b.v., Hilversum, The Netherlands). Briefly, Huygens is an iterative program that encodes light as 32-bit gray levels and reassigns it at high probability to specific voxels in the stack using a point spread function. This results in removing fuzziness contained in the stack. In the present study, the maximum likelihood estimation algorithm was used throughout (24, 25). Restored stacks were then further processed with Imarys (BitPlane, Zurich, Switzerland) for visualization and volume rendering. Huygens and Imarys programs were run on a four-processor Origin 2000 and a two-processor Octane (SGI), respectively.

Time-lapse Video Microscopy—For living cell studies, a laboratory made device maintained cells in a 37 °C, 5% CO₂, >80 relative humidity atmosphere. Epifluorescence illumination was ensured by a halogen light bulb (100 watts). GFP positive cells grown on 0.17-mm-thick glass coverslip were studied 18 h after transfection with an inverted DMIRBE using a 63× (numeric aperture, 1.32). Cell images were captured (exposure time, 400 ms) every 10 s for 10 min as time series of 16-bit files. For video presentation, selected images were cropped, assembled, and compressed using Quicktime (version 4.0).

Scanning Electron Microscopy (SE)—Transfected REF-52 cells were grown on glass coverslips, fixed in 0.1 M sodium cacodylate (pH7.2) containing 2% glutaraldehyde and 0.1 M sucrose for at least 1 h, and processed for SE as described (26). Samples were observed using a Hitachi S4000 scanning microscope at 15 kV. For all experiments, at least 50 cells were examined. Images were processed as above. To estimate the fraction of transfected cells, one coverslip was processed for F-actin, TCL_{Q79L}, and TC10_{Q75L} detection by immunofluorescence. In all experiments, the same proportion of cells with altered morphology was observed either by SE or immunohistochemistry.

RESULTS

Characterization of TCL, a TC10-like Protein—A general survey of nucleotide sequences encoding new GTPases of the Rho family was performed in human and murine expressed sequence tag (EST) data bases. We isolated a set of 16 human and 14 murine EST sequences with 70% identity to human or murine TC10 ORF (27). These sequences showed lower levels of identity with Cdc42, RhoG, or Rac1. Merging overlapping ESTs produced a 2,195-bp human and a 2,252-bp murine consensus cDNA sequences, whose ORFs were 87% identical. ORFs from both species were PCR-amplified from IMAGE clones 269952 and 316263, respectively, and fully sequenced (accession numbers AJ276567 and AJ276568). Human and murine ORFs potentially encode 214 and 204 amino acids proteins, respectively, that share 95% sequence similarity (93% identity), all changes being clustered within the amino-terminal and carboxyl-terminal ends. These proteins contain the canonical G1–3 boxes involved in the nucleotide binding and conserved among Ras-like GTPases, as well as a two-cysteine “CCAAX” box, a substrate for geranylgeranyl- and farnesyltransferases. Protein sequence alignment with other GTPases of the Rac/Cdc42 subfamily showed that, like TC10, these proteins contain an amino-terminal extension compared with Cdc42, Rac, or RhoG, which differs in length between man and mouse (Fig. 1A). Sequence alignment of human Rho proteins was next used to compute pairwise similarity matrixes and to draw a similarity dendrogram, which clearly showed that the new protein shares a significant stem with TC10 (Fig. 1B). For these reasons, this protein will be referred to as TCL (TC10-like).

TCL Gene Structure—Data base search also revealed significant matches within a 169,645-bp genomic fragment from human chromosome 14 (AL049871.2, Genoscope, France). Further analysis showed that this fragment contains all genomic counterparts of whole of TCL cDNA sequence (Fig. 2). The human TCL gene is made of 5 exons, the first one (39,379–40,011) encoding the 5'-untranslated region and the first 59 amino acids. The second exon (102,071–102,132) encodes amino acids 60–79 and is separated by an unusually long intron (62,061 bp) from the first exon. Exon 3 (113,934–

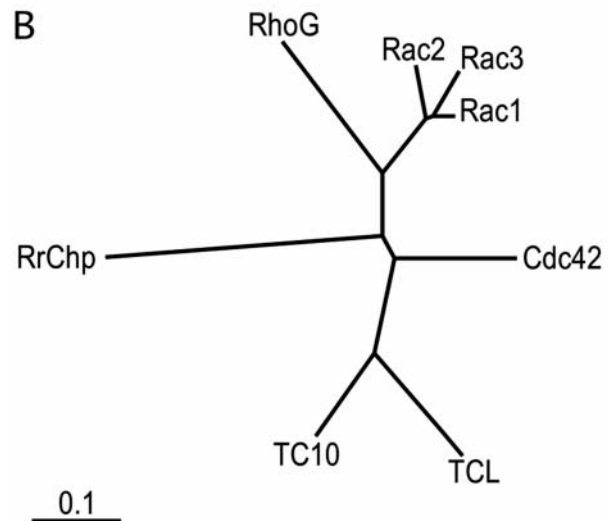
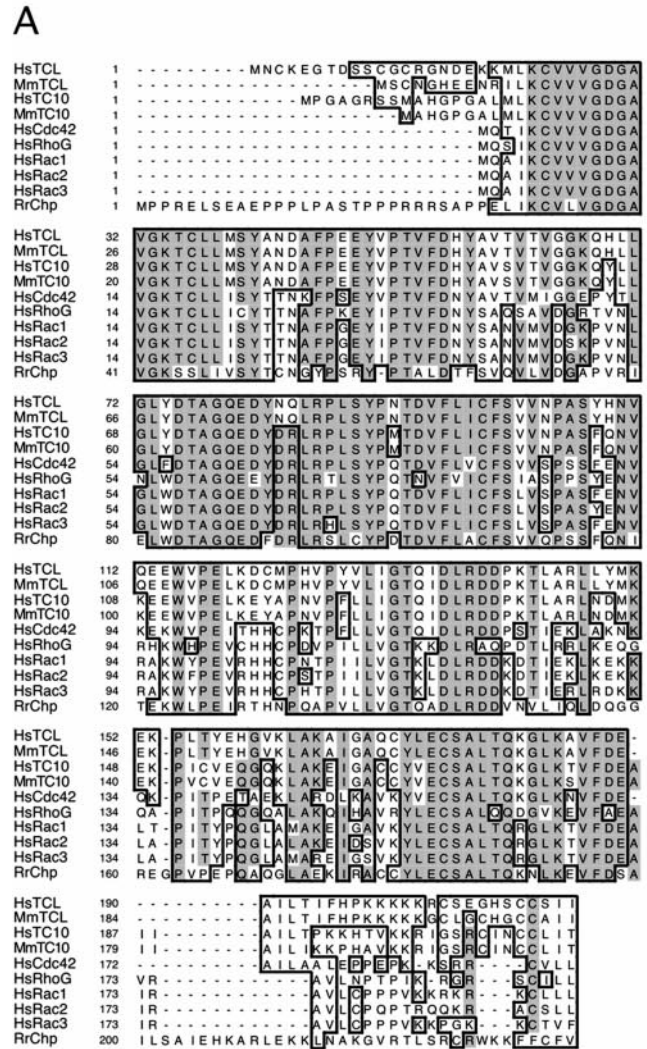


FIG. 1. Comparison of TCL protein with other Rho proteins. A, human and mouse TCL protein sequences were aligned with human and mouse TC10, human Cdc42, RhoG, Rac1, Rac2, Rac3, and rat Chp using Multalin (19). Identical residues are shaded, and conserved residues are boxed. Numbering refers to the published sequences. B, a similarity tree was drawn from distances computed from alignment of human protein sequences using ClustalW and Treeview (20, 21). The bar length at the bottom represents 10% divergence.

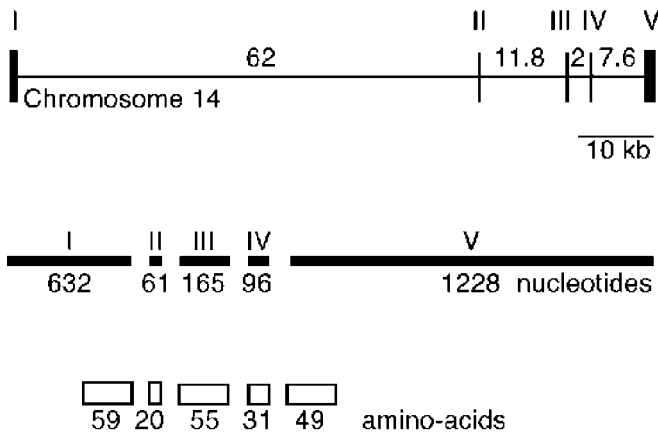


FIG. 2. Schematic representation of human TCL gene structure. TCL exons (I–V) on chromosome 14 are represented by vertical bars on top of the figure. Intron lengths are expressed as kilobase pairs. For each TCL exon, size (middle panel) as well as number of encoded amino acids (bottom panel) are indicated.

114,099) encodes amino acids 80–134, exon 4 (116,082–116,178) encodes amino acids 135–165, and exon 5 (123,839–125,067) amino acids 166–214. Thus, the human TCL gene represents the largest gene encoding a Rho GTPase characterized so far, spanning over 86 kb.

Tissue Specificity of TCL mRNA Expression—We next examined the pattern of expression of TCL mRNA. To this aim, we used a 1.7-kb probe derived from the original IMAGE 316263 murine clone, covering the 5'-untranslated region, the ORF, and two thirds of the 3'-untranslated region. Hybridization of the TCL probe to a Northern blot membrane from multiple mouse tissues revealed the presence of a single mRNA product of about 2.5 kb (Fig. 3). This is in consistency with 2,252-bp length of the consensus sequence (excluding the poly(A) tract), merged from the various murine TCL ESTs. TCL mRNA is expressed at high levels in heart, and at moderate levels in lung and liver. Very low levels could be detected in the other tissues. TCL pattern of expression differs from TC10 and Cdc42. TC10 has been reported to be expressed at high levels in heart and skeletal muscle but at very low levels in other tissues such as lung and liver, while Cdc42 is expressed at moderate levels in most tissues (9).

Biochemical Properties of TCL—We next purified wild-type TCL and TC10 deleted from their CAAX boxes as GST fusions in bacteria and compared their biochemical properties. We first examined the kinetics of [³⁵S]GTP γ S and [³H]GDP loading of TCL. Since the recombinant protein was purified in the presence of GDP, GDP dissociation represents the first and the rate-limiting step. The increase in TCL bound to labeled nucleotides therefore reflects the dissociation of the original bound GDP. At 37 °C and in a physiological buffer containing 2 mM MgCl₂, TCL bound [³⁵S]GTP γ S and [³H]GDP at the same rate ($t_{1/2} = 2$ min) (Fig. 4A). Assuming single-exponential kinetics, TCL dissociates from GDP at an apparent rate of $0.34 \pm 0.05 \text{ min}^{-1}$. Fig. 4B shows GTP γ S dissociation kinetics of TCL and TC10. GTPases were first loaded with [³⁵S]GTP γ S in low magnesium buffer and then allowed to dissociate from the labeled nucleotide by incubation at 37 °C with 2 mM Mg²⁺ and 1 mM cold GTP. Under these conditions, TCL dissociated from GTP γ S with a k_{off} approximating $0.085 \pm 0.01 \text{ min}^{-1}$, while TC10 showed a slower dissociation rate ($k_{\text{off}} = 0.055 \pm 0.008 \text{ min}^{-1}$). These k_{off} are higher than values previously determined at 30 °C for TC10 ($0.006\text{--}0.018 \text{ min}^{-1}$) (9, 28). Fig. 4C shows the basal GTPase activity of TCL and TC10. GTPases were loaded with [γ -³²P]GTP in low magnesium, and the release of ³²P_i was measured at 37 °C after 2 mM Mg²⁺ addition.

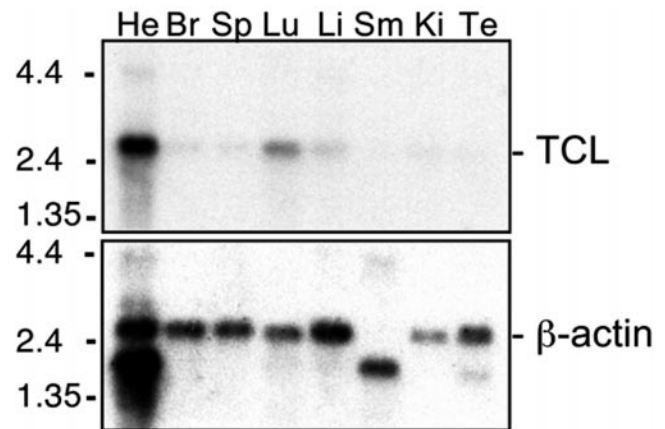


FIG. 3. TCL mRNA distribution in murine tissues. Mouse Multiple Northern Tissues membrane (CLONTECH) was sequentially hybridized with ³²P-labeled full-length TCL and β -actin cDNA probes. *He*, heart; *Br*, brain; *Sp*, spleen; *Lu*, lung; *Li*, liver; *Sm*, skeletal muscle; *Ki*, kidney; *Te*, testis. Membranes were exposed for 12 h (TCL) and for 4 h (β -actin). Sizes (in kilobases) are indicated on the left.

Under these conditions, TCL hydrolyzed 7% of its bound GTP per minute, while TC10 hydrolyzed 5% of it. These values are in the range of those reported for TC10 hydrolysis at 37 °C (0.06 min^{-1}) (28).

Active TCL Interacts with PAK and WASP—As mentioned above, TCL and TC10 protein sequences are highly similar in their amino-terminal region, and are strictly conserved in their effector loop (HsTCL amino acids 48–59, Fig. 1A). To evaluate whether TCL can bind targets containing a CRIB domain as TC10 does, we first generated TCL mutants expected to be preferentially loaded with GTP or GDP. To produce a constitutively active TCL protein, glutamine 79 was replaced by leucine (Q79L). This substitution is equivalent to the classical Q61L mutation previously shown to reduce the overall GTP hydrolysis rate in other Rho GTPases (reviewed in Ref. 27). We also replaced threonine 35 by an asparagine (T35N), whose equivalent substitution in Ras (T17N) has been reported to lock the GTPase in the GDP-bound form (30). Both mutants were expressed as LexA fusions and assayed for interaction with PAK-1 and with the CRIB domain of WASP fused to Gal4. As shown in Fig. 5A, a high β -galactosidase activity was detected when LexA-TCL_{Q79L} was co-expressed with GalAD-PAK-1 or GalAD-WASP. Similar levels of β -galactosidase activity were observed when LexA-TC10_{Q75L} or LexA-Cdc42_{G12V} were expressed, while RhoG_{G12V} did not show any interaction. Yeasts co-expressing LexA-TCL_{T35N} failed to produce any β -galactosidase activity, indicating that only the GTP-bound form of TCL binds PAK-1 and WASP. Similar levels of expression were detected for Cdc42, TC10, and TCL constructs in yeast extracts (Fig. 5A, lower panel). As a negative control, we co-expressed GalAD fused to a kinectin fragment, which specifically binds to RhoG_{G12V} and Rac1_{G12V} (16). This fragment failed to produce any interaction with TCL_{Q79L}, TC10_{Q75L}, and Cdc42_{G12V} fusions. The interaction of GTP-bound TCL was confirmed in mammalian cells using a CRIB affinity assay (23) (Fig. 5B). Lysates from Bosc cells expressing GFP or GFP fused to Cdc42_{G12V}, RhoG_{G12V}, TC10_{Q75L}, or TCL_{Q79L} were incubated with GST-CRIB_{PAK} bound to Sepharose beads. Western blotting analysis of bound proteins using an anti-GFP antibody shows that GFP-Cdc42_{G12V}, GFP-TC10_{Q75L}, and GFP-TCL_{Q79L} were efficiently bound, whereas GFP or GFP-RhoG_{G12V} proteins were not (Fig. 5B, upper panel). As a control, lysates from GFP-TCL_{Q79L}-expressing cells were incubated in the presence of GST (Fig. 5B, last lane), which produced no interaction. The presence of wild-type and fusion GFP in total lysates was checked

FIG. 4. Biochemical properties of *E. coli* expressed GST-TCL protein. *A*, kinetics of GDP and GTP γ S binding on TCL (25 pmol/point) at 37 °C in 2 mM Mg²⁺. *B*, kinetics of GTP γ S dissociation from TCL and TC10 at 37 °C in 2 mM Mg²⁺ with 1 mM GTP as competitor. *C*, GTP hydrolysis by TCL and TC10 proteins at 37 °C in 2 mM Mg²⁺.

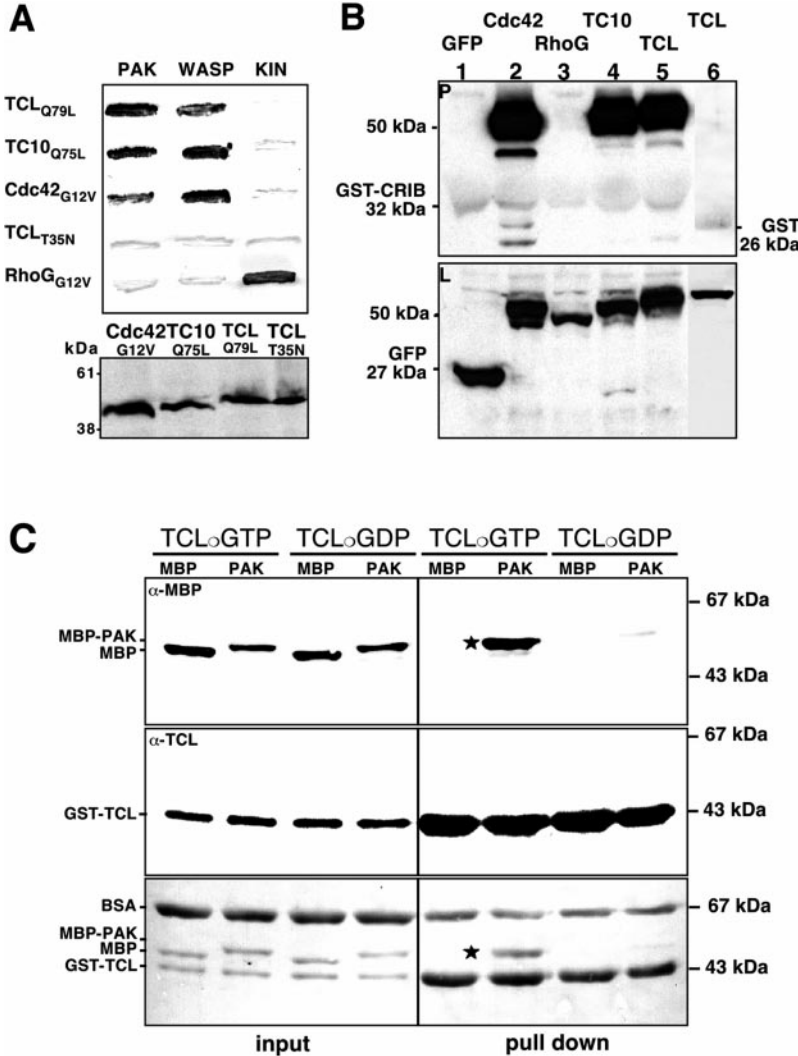
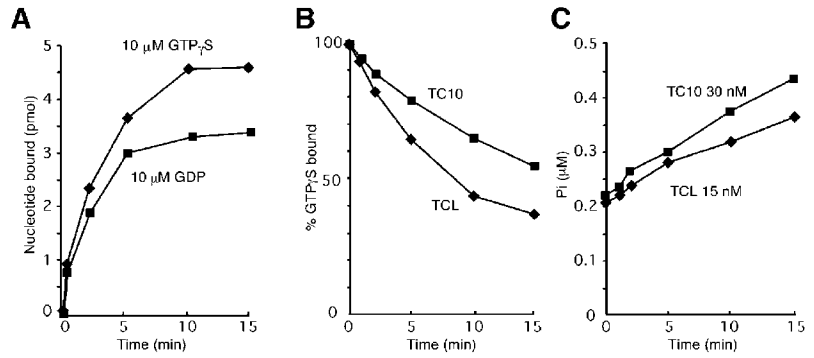


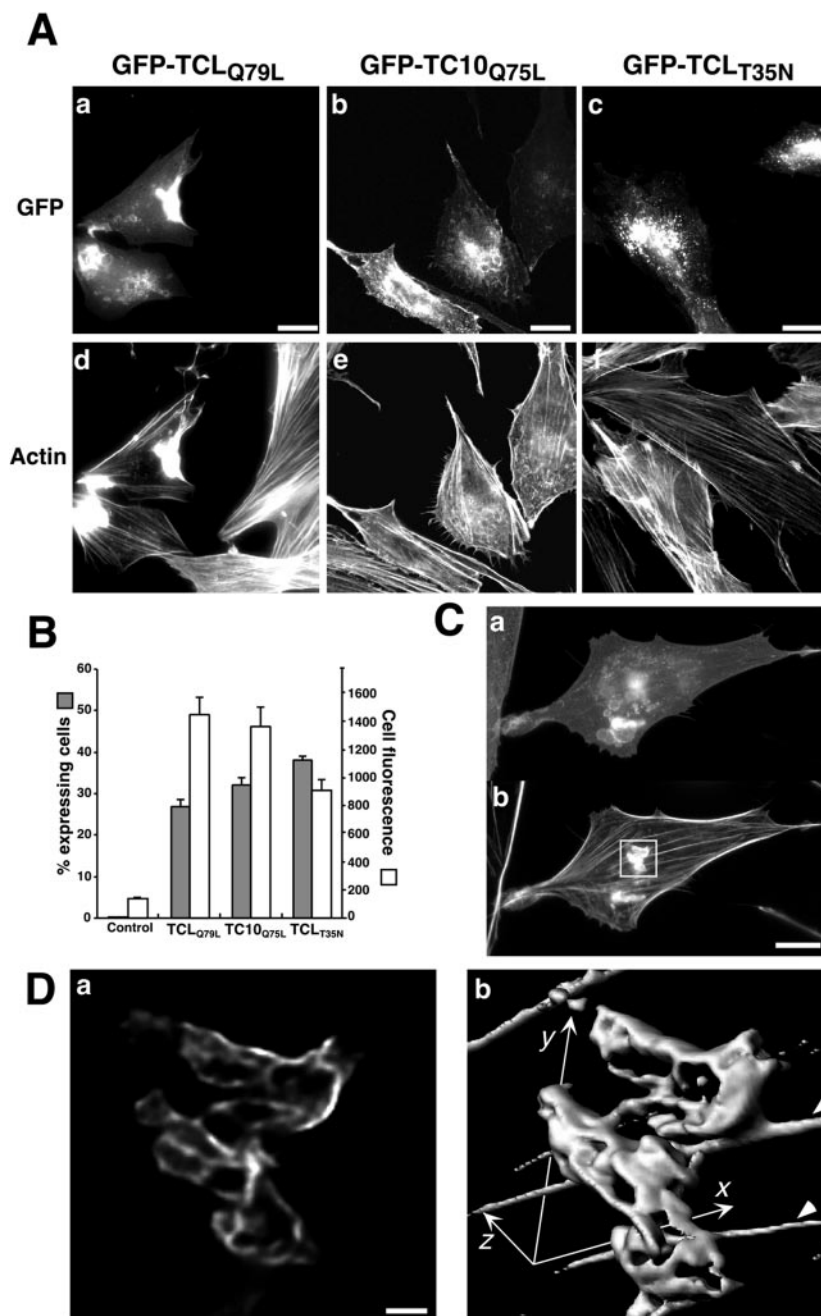
FIG. 5. GTP-bound TCL binds CRIB domains. *A*, two-hybrid analysis. *Upper panel*, TAT-7 yeast strain was cotransformed with plasmids allowing the expression of LexA fused to GTP-bound TCL_{Q79L}, TC10_{Q75L}, Cdc42_{G12V}, RhoG_{G12V}, or GDP-bound TCL_{T35N}, and Gal4 activation domain fused to PAK, WASP, or kinecin (*KIN*). Double transformants were selected and assayed for β -galactosidase activity as described under “Experimental Procedures.” *Lower panel*, Western blot analysis of yeast extracts expressing active GTPases fused to LexA. The membrane was revealed using an anti-LexA antibody. *B*, CRIB affinity precipitation. Human Bosc cells were transfected with plasmids allowing the expression of GFP alone or fused to various activated GTPases. Cell lysates were precipitated with GST-CRIB immobilized on glutathione-Sepharose 4B beads (23). Alternately, lysate from cells expressing TCL_{Q79L} (lane 6) were precipitated with control GST-bound beads. GST-CRIB-bound (lanes 1–5) or GST-bound (lane 6) proteins from 10⁶ cells (panel P) and total cell lysate from 10⁴ cells (panel L) were analyzed by Western blotting for GFP expression. *C*, direct interaction between TCL.GTP and CRIB domains. Sepharose-bound GST-wTCL (10 μg/lane) was loaded with GDP or GTP and bound to 15 μg of affinity-purified MBP or MBP fused to the CRIB domain of PAK (MBP-PAK). The level of input proteins (left panel) and GST-TCL bound proteins (right panel) was controlled by Western blotting revealed by anti-MBP antibodies (upper panels), anti-TCL antibodies (middle panels), and Ponceau staining (lower panels). The presence of MBP-PAK in TCL-GTP-bound proteins is indicated by a star.

by Western blotting, which showed that all constructs had been expressed at comparable levels (Fig. 5*B*, lower panel). To establish that TCL directly interacts with CRIB domains, affinity-purified MBP fused to CRIB_{PAK} was incubated with glutathione beads bound to GST-TCLwt loaded with GDP or GTP. Fig. 5*C* shows that TCL.GTP efficiently interacted with MBP-CRIB_{PAK}, while barely detectable levels were observed with TCL.GDP (upper and lower right panels). MBP alone produced no interaction with either form of TCL. The amount of input and pulled-down purified proteins was controlled by Western blotting using anti-MBP and anti-GST antibodies (upper and middle panels) and by Ponceau staining (lower panel). These experiments therefore establish that TCL efficiently and directly binds CRIB domains.

Active TCL Modifies the Actin Cytoskeleton of REF-52 Cells—

Previous studies have established that expression of TC10_{Q75L} produces numerous peripheral filopodial extensions and a reduction in the level of stress fibers, a phenotype similar but exaggerated compared with that of Cdc42_{G12V} (9). We thus looked for differential morphogenic activity of TCL_{Q79L} in REF-52 fibroblastic cells. To this aim, TCL_{Q79L} and TC10_{Q75L} were expressed as carboxyl-terminal fusions with the GFP and the distribution of F-actin was examined. 100% of cells expressing GFP-TCL_{Q79L} (Fig. 6*A*, panel a) displayed strong and localized F-actin accumulation (panel d), as well as an overall reduction in actin stress fibers. In 40% transfected cells, a low number of thin F-actin-rich peripheral extensions were observed (<10/cell) (see Fig. 6*C*). In comparison, about 80% of cells expressing GFP-TC10_{Q75L} (panel b) produced numerous

FIG. 6. Cytoskeletal effects of active TCL. **A**, rat REF-52 fibroblasts were transfected with plasmids allowing the expression of GFP fused to TCL_{Q79L} (panels *a* and *d*), TC10_{Q75L} (panels *b* and *e*), and TCL_{T35N} (panels *c* and *f*). 18 h after transfection, cells were fixed and examined for GFP fluorescence (panels *a–c*) and F-actin distribution (panels *d–f*). For each panel set, at least 100 independent expressing cells were analyzed. Bar, 10 μ m. **B**, transfection and relative expression efficiency of GFP constructs. 18 h after transfection, the fraction of GFP-positive cells was measured from three independent experiments by examining a 100-cell population (shaded bars). GFP intensities were quantified from a 400-ms exposure time images on at least 50 positive cells using the MetaMorph program (open bars). Values correspond to the average of 12-bit encoded integrated fluorescence levels of expressing cells. Error bars represent S.E. values. **C**, TCL_{Q79L} expressing REF-52 used for image deconvolution and volume rendering. The cell was visualized for GFP (panel *a*) and stained for F-actin (panel *b*). The actin structure used for image processing is boxed. Bar, 10 μ m. **D**, detailed analysis of TCL-dependent actin structures. Panel *a*, optical section of the actin structure boxed in **C**. A stack of 80 optical sections (z step = 0.088 μ m) was deconvolved using the Huygens system. Shown is a processed optical section located at 4.7 μ m above the stress fibers plane. Bar, 1 μ m. Panel *b*, volume rendering of the actin structure boxed in **C**. Deconvolved images were processed with Imaris 3.0 (BitPlane). (x , y , z) represents original coordinate axes of the image stack. Arrowheads indicate stress fibers.



filopodial extensions (>30/cell) associated with a reduction in actin stress fibers and the presence of F-actin dots, which might correspond to small protrusions on the dorsal membrane (panel *e*). We also examined the effects of GFP-TCL_{T35N} expression (panel *c*). All expressing cells maintained a morphology similar to control cells but showed a slight but significant increase in actin stress fibers (panel *f*), suggesting that this mutant indeed behaves as a dominant inhibitor. The phenotypic differences observed between TCL_{Q79L} and TC10_{Q75L} were not a consequence of differential expression, since comparable efficiencies of transfection and expression were obtained for all constructs (Fig. 6B). To further characterize F-actin structures elicited by TCL_{Q79L} expression, images of a TCL-expressing cell region were acquired at different focusing planes and processed for deconvolution and volume rendering. A deconvolved section at 4.7 μ m above the stress fiber plane clearly showed that the strong F-actin signal observed on the cell shown in Fig. 6C (boxed in panel *b*) is distributed according

to a ruffle pattern (Fig. 6D, panel *a*). This was better evidenced by volume rendering (Fig. 6D, panel *b*), which showed that the overall structure adopts a ruffle morphology.

Effects of Active TCL on Cell Morphology—To compare the effects of TCL_{Q79L} and TC10_{Q75L} expression on cell morphology, we next analyzed transfected cells by scanning electron microscopy (Fig. 7). More than 40% of cells (which would correspond to at least 80% of TCL_{Q79L} expressing cells) displayed an elongated morphology, with a low number of long and thin extensions at their periphery (panel *a*). Most cells exhibited one to three large protrusions on the dorsal membrane (boxed in panel *a* and 8-fold enlarged in panel *c*). These dorsal structures show a shape very similar to the one obtained after volume rendering of F-actin structures (see Fig. 6D, panel *b*). By comparison, cells expressing TC10_{Q75L} (Fig. 7, panel *b*) displayed a motile cell morphology, associated with the formation of numerous filopodia. A reduced number of wormlike structures was observed on the dorsal membrane, in consistency with the

F-actin staining (Fig. 6A, panel e). Identical overall level of expression were observed for both constructs, as monitored by Western blotting (Fig. 7, panel d) and epifluorescence analysis (data not shown). To get an insight in the way TCL- and TC10-dependent structures are dynamically regulated, we analyzed expressing cells by time-lapse videomicroscopy (see Supplemental Material). TCL_{Q79L}-expressing cells exhibited a limited number (average 2.2 ± 0.5 , $n = 27$) of very dynamic dorsal ruffles whose activity appeared associated with the formation of large cytoplasmic vesicles. In contrast, TC10 produced an average of $6.5 (\pm 1.2)$, $n = 15$ dynamic peripheral flat protrusions in which 5–10 filopodia showed back and forth elongation. Although small lamellipodia were occasionally observed, dorsal structures or cytoplasmic vesicles were never detected in TC10_{Q75L}-expressing cells. These data confirm that, although

sharing a high similarity in their primary structures, TCL_{Q79L} and TC10_{Q75L} elicit different effects on cell morphology.

Dominant Negative Rac1 and Cdc42 Inhibit TCL Activity—The presence of dorsal structures in TCL_{Q79L}-expressing cells prompted us to examine whether Rac1 and Cdc42 might participate to the establishment of TCL phenotype (Fig. 8). To this aim, we coexpressed in REF-52 cells GFP-TCL_{Q79L} (panels a and d) with Myc-tagged Rac1_{T17N} (panel b) or Cdc42_{T17N} (panel e). These mutants have been previously shown to act as inhibitors of endogenous Rac1 and Cdc42 activities (reviewed in Ref. 1). As observed on panel c, cells coexpressing TCL_{Q79L} and Rac1_{T17N} still displayed an elongated shape, but maintained a high level of actin stress fibers and were devoid of ruffles on the dorsal membrane. Cells coexpressing TCL_{Q79L} and Cdc42_{T17N} (panel f) were also devoid of ruffles and maintained a high stress fiber content. As a control, cells coexpressing GFP-TCL_{Q79L} and Myc-tagged Rac1_{wt} (panels g and h) still showed a reduced stress fiber content and elicited the formation of dorsal ruffles. Expression of Myc-tagged Rac1 and Cdc42 alone had no effect on F-actin distribution (data not shown), as reported previously (16, 22). This indicates that coexpression of the dominant negative versions of Rac1 and Cdc42 inhibit the establishment of TCL_{Q79L} phenotype.

DISCUSSION

The Rho family of GTPases represents a group of more than fifteen proteins sharing at least 50% identity in their amino acid sequence. These proteins have been shown to control many aspects of cell physiology, including the formation of dynamic F-actin rich structures, cell proliferation, and apoptosis, as well as cell transformation. The initiation of these cellular events is mediated by guanine nucleotide exchange factors, acting upstream of the GTPases (31), and by protein kinases, lipid kinases, coiled-coil proteins, and transcription factors, acting downstream of the GTPases (15). Rho proteins have been shown to display different patterns of tissular expression, and to exert their effects through a coordinated network of regulation. Here we report the identification of TCL, a new member of the Rho family more closely related to TC10 and Cdc42. We found that TCL is encoded by an unusually large gene located on human chromosome 14 and shows high levels of mRNA expression in heart. As far as the protein is concerned, the dominant active TCL protein binds to the same CRIB-containing effectors as TC10 and Cdc42. Despite this similarity, expression of the dominant active TCL in fibroblastic cells exhibits unique features, eliciting the formation of F-actin-rich structures on the dorsal membrane, sensitive to Rac1 and Cdc42 inhibition.

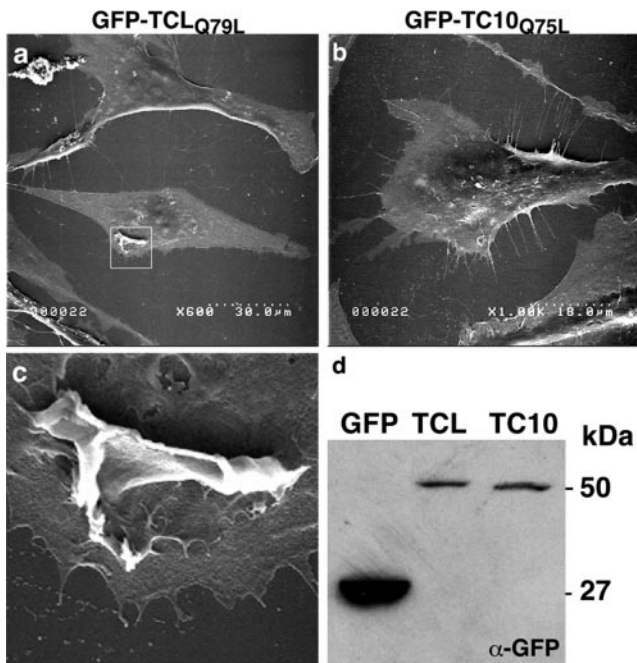
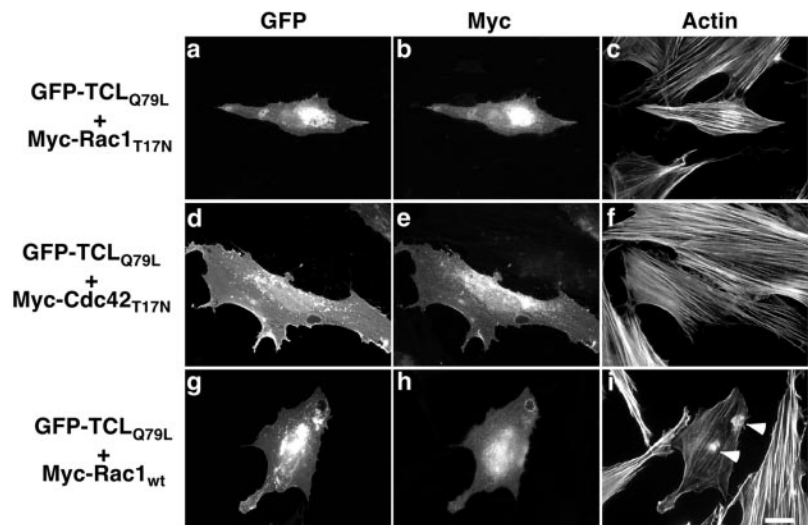


FIG. 7. Morphogenic effects of active TCL. REF-52 cells expressing GFP-TCL_{Q79L} (panel a; original magnification, $\times 600$) or GFP-TC10_{Q75L} (panel b; original magnification, $\times 1000$) were examined under SE. Panel c shows the membrane protrusion boxed in panel a at higher magnification ($\times 4800$). Control transfected cell coverslips were monitored for GFP expression by Western blotting using an anti-GFP antibody (panel d) and by immunofluorescence. For panels a–c, more than 100 cells were analyzed.

FIG. 8. TCL morphogenic activity is inhibited by dominant negative Rac1 and Cdc42. REF-52 cells were co-transfected with constructs allowing the expression of GFP-TCL_{Q79L} and Myc-tagged Rac1_{T17N} (panels a–c), Myc-tagged Cdc42_{T17N} (panels d–f), or Myc-tagged Rac1_{wt} (panels g–i). 18 h after transfection, cells were fixed and observed for GFP fluorescence (panels a, d, and g), Myc epitope expression (panels b, e, and h) and F-actin distribution (panels c, f, and i). Arrowheads in panel i show the position of dorsal ruffles. Bar, 10 μ m.



The identification of TCL originated from a global search in nucleic acids data bases for expressed cDNA sequence tags encoding new GTPases of the Rho family. Although we also searched for sequences similar to human Rac1, Cdc42, RhoG, TC10, Chp, and RhoA, only TCL sequence was recovered as a new Rho GTPase. This might reflect a situation in which nearly all sequences encoding Rho GTPases have been now determined. However, a limited number of Rho-encoding mRNAs might still remain unknown that are either expressed at very low levels or in tissues not used for constructing cDNA libraries. Indeed, although we found many ESTs for other Rho proteins, only two sequences homologous to Chp (32) were found in the human EST data base and none in the murine data base. Human genomic data base search revealed that TCL gene is located on chromosome 14 and is made of five exons, spanning over 86 kb. This represents an unusually large locus for a Ras-like GTPase. Indeed, Ras-like genes identified so far span from 4 kb (Ha-, Ki-, N-, and R-Ras) to 25 kb (RhoG) (33). The human TCL gene might be even larger, since most Ras-like genes contain a 5' non-coding exon (34). Nevertheless, analysis of the genomic sequences upstream of the first exon did not identify transcription regulatory elements such as TATA or CAAT boxes nor polypyrimidine tracts usually found in the 3' end of intronic sequences. Instead, it revealed the presence of three ESTs unrelated to TCL (AL039470, AL039471, and AI698602) corresponding to a distinct transcription unit located 5 kb upstream of TCL. These data suggest that the promoting sequences of TCL gene should not lie farther than 5 kb upstream of the first exon.

The characterization of TCL as a new protein closely related to TC10 and Cdc42 raises the question as to whether these members control distinct or redundant pathways. We observed that TCL is preferentially expressed in heart, while TC10 is expressed at high levels in heart and skeletal muscle, Cdc42 being ubiquitously distributed (9). Our data also demonstrate that TCL has the ability to bind the same CRIB-containing effectors as TC10 and Cdc42. Thus, the comparison of their respective tissue expression and downstream effectors would rather call for a functional redundancy between TCL and TC10. As far as biochemical activities are concerned, our data show that TCL exhibits dissociation and hydrolysis rates both 40% higher than TC10. In addition, TCL rapidly exchanges GDP for GTP. This suggests that wild-type TCL might be predominantly bound to GTP *in vivo*, unless down-regulated by a GTPase-activating protein. This supports our observations that overexpression of wild-type TCL induces the same phenotypic changes as TCL_{Q79L}, although at a lower efficiency (data not shown).

Despite the similarities between TCL and TC10, we observed striking differences in their cellular effects. Whereas TC10_{Q75L} expression produces numerous filopodial extensions and microvilli, TCL_{Q79L}-expressing cells show a limited number of ruffle-like protrusions on their dorsal membrane associated with large intracytoplasmic vesicles (see videos in Supplemental Materials). How so closely related proteins might produce so distinct effects in the same cell system remains an open question. One possibility is that, although TC10 and TCL efficiently bind CRIB domains, they might still activate distinct CRIB-containing proteins. A similar situation has been reported for Borg-3, a CRIB protein that binds to Cdc42 but not to TC10 (9). A second possibility is that the functional differences between TCL and TC10 rely on different subcellular localizations. Indeed, TC10 protein accumulates in the perinuclear area, whereas TCL displays a more diffuse distribution, reminiscent of Rac1 localization.

We show that TCL activity is inhibited upon expression of dominant negative Rac1_{T17N} and Cdc42_{T17N}. T17N mutants are thought to inhibit endogenous GTPase activity by titrating

their respective exchange factors (30). Their inhibitory effect on TCL activity might be explained by two distinct mechanisms. On the one hand, given the high amino acid similarity between Cdc42 and TCL, both proteins might share regulatory factors, which could be directly inhibited by Cdc42_{T17N}. Our preliminary data suggest that several exchange factors might indeed activate both proteins *in vitro*. On the other hand, the inhibitory effect of Cdc42_{T17N} might indicate that Cdc42 activity is required downstream of TCL. This is also probably the case for Rac1, since TCL_{Q79L} promotes the formation of ruffles and intracytoplasmic vesicles, a feature shown to be under the control of Rac1 (35). A similar situation has been reported for Cdc42, which produces filopodia but also promotes the formation of Rac1-dependent lamellipodia (6).

In conclusion, our data describe TCL as a new protein related to TC10 and Cdc42 that controls the formation of distinct cytoskeletal structures. Identifying exchange factors as well as downstream targets should help elucidating the mechanisms by which TCL exerts its morphogenic activity.

Acknowledgments—We thank Dr. P. Travo, head of the Centre de Recherche en Biochimie Macromoléculaire Integrated Imaging Facility, for constant interest and support. We are indebted to P. Chardin and S. Paris for help in biochemical analysis. We thank P. Roux, M. Pucéat, M. Mérianne, and S. Mary for fruitful discussion. We also thank John Collard for the gift of GST-PAK construct.

REFERENCES

- Kjoller, L., and Hall, A. (1999) *Exp. Cell Res.* 253, 166–179
- Keely, P., Parise, L., and Juliano, R. (1998) *Trends Cell Biol.* 8, 101–106
- Fort, P. (1999) in *Progress in Molecular and Subcellular Biology* (Jeanteur, P., ed) Vol. 22, pp. 159–181, Springer-Verlag, Berlin
- Aspenström, P. (1999) *Exp. Cell Res.* 246, 20–25
- Ridley, A. J. (1994) *BioEssays* 16, 321–327
- Tapon, N., and Hall, A. (1997) *Curr. Opin. Cell Biol.* 9, 86–92
- Murphy, C., Saffrich, R., Grummt, M., Gournier, H., Rybin, V., Rubino, M., Auvinen, P., Lutcke, A., Parton, R. G., and Zerial, M. (1996) *Nature* 384, 427–432
- Nobes, C. D., and Hall, A. (1995) *Cell* 81, 53–62
- Neudauer, C. L., Joberty, G., Tatsis, N., and Macara, I. G. (1998) *Curr. Biol.* 8, 1151–1160
- Gallo, G., and Letourneau, P. C. (1998) *Curr. Biol.* 8, 80–82
- Reif, K., and Cantrell, D. A. (1998) *Immunity* 8, 395–401
- Stowers, L., Yelon, D., Berg, L. J., and Chant, J. (1995) *Proc. Natl. Acad. Sci. U. S. A.* 92, 5027–5031
- Gomez, J., Martinez, A. C., Gonzalez, A., and Rebollo, A. (1998) *Immunol. Cell Biol.* 76, 125–134
- Boguski, M. S., and McCormick, F. (1993) *Nature* 366, 643–654
- Aspenström, P. (1999) *Curr. Opin. Cell Biol.* 11, 95–102
- Gauthier-Rouvière, C., Vignal, E., Mérianne, M., Roux, P., Montcourier, P., and Fort, P. (1998) *Mol. Biol. Cell* 9, 1379–1394
- Moorman, J. P., Luu, D., Wickham, J., Bobak, D. A., and Hahn, C. S. (1999) *Oncogene* 18, 47–57
- Altschul, S. F., Gish, W., Miller, W., Myers, E. W., and Lipman, D. J. (1990) *J. Mol. Biol.* 215, 403–410
- Corpet, F. (1988) *Nucleic Acids Res.* 16, 10881–10890
- Thompson, J. D., Higgins, D. G., and Gibson, T. J. (1994) *Nucleic Acids Res.* 22, 4673–4680
- Page, R. D. (1996) *Comput. Appl. Biosci.* 12, 357–358
- Blangy, A., Vignal, E., Schmidt, S., Debant, A., Gauthier-Rouvière, C., and Fort, P. (2000) *J. Cell Sci.* 113, 729–739
- Sander, E. E., van Delft, S., ten Klooster, J. P., Reid, T., van der Kammen, R. A., Michiels, F., and Collard, J. G. (1998) *J. Cell Biol.* 143, 1385–1398
- van der Voort, H. T. M., and Straters, K. C. (1995) *J. Microsc.* 178, 165–181
- van der Voort, H. T. M., Messerli, J. M., Noordmans, H. J., and Smeulders, A. W. M. (1993) *Bioimaging* 1, 20–29
- Brunk, U., Collins, V. P., and Arro, E. (1981) *J. Microsc.* 123, 121–131
- Drivas, G. T., Shih, A., Coutavas, E., Rush, M. G., and D'Eustachio, P. (1990) *Mol. Cell Biol.* 10, 1793–1798
- Murphy, G. A., Soliski, P. A., Jillian, S. A., Perez de la Ossa, P., D'Eustachio, P., Der, C. J., and Rush, M. G. (1999) *Oncogene* 18, 3831–45
- Hall, A. (1998) *Science* 279, 509–514
- Feig, L., and Cooper, G. M. (1988) *Mol. Cell Biol.* 8, 3235–3243
- Stam, J. C., and Collard, J. G. (1999) in *Progress in Molecular and Subcellular Biology* (Jeanteur, P., ed) Vol. 22, pp. 51–83, Springer-Verlag, Berlin
- Aronheim, A., Broder, Y. C., Cohen, A., Fritsch, A., Belisle, B., and Abo, A. (1998) *Curr. Biol.* 8, 1125–1128
- Courjal, F., Chuchana, P., Theillet, C., and Fort, P. (1997) *Genomics* 44, 242–246
- Le Gallic, L., and Fort, P. (1997) *Genomics* 42, 157–160
- Ridley, A. J., Paterson, H. F., Johnston, C. L., Diekmann, D., and Hall, A. (1992) *Cell* 70, 401–410

Characterization of TCL, a New GTPase of the Rho Family related to TC10 and Cdc42

Emmanuel Vignal, Marion De Toledo, Franck Comunale, Angela Ladopoulou, Cécile Gauthier-Rouvière, Anne Blangy and Philippe Fort

J. Biol. Chem. 2000, 275:36457-36464.

doi: 10.1074/jbc.M003487200 originally published online August 30, 2000

Access the most updated version of this article at doi: [10.1074/jbc.M003487200](https://doi.org/10.1074/jbc.M003487200)

Alerts:

- [When this article is cited](#)
- [When a correction for this article is posted](#)

[Click here](#) to choose from all of JBC's e-mail alerts

Supplemental material:

<http://www.jbc.org/content/suppl/2000/11/15/275.46.36457.DC1>

This article cites 35 references, 7 of which can be accessed free at <http://www.jbc.org/content/275/46/36457.full.html#ref-list-1>